Journal of Physical Chemistry, accepted (2009)

Theoretical Characterization of the Structural and Hole Transport Dynamics in Liquid-Crystalline Phthalocyanine Stacks

Y. Olivier[1], L. Muccioli[2], V. Lemaur[1], Y.H. Geerts[3], C. Zannoni[2], and J. Cornil[1]

[1]*Laboratory for Chemistry of Novel Materials*
University of Mons-Hainaut,
Place du Parc 20, BE-7000 Mons, Belgium

[2]*Dipartimento di Chimica Fisica e Inorganica and INSTM*
Università di Bologna
Viale Risorgimento 4, IT-40136 Bologna, Italy

[3]*Laboratoire de Chimie des Polymères,*
Faculté des Sciences,
Université Libre de Bruxelles, ULB, CP 206/01,
Boulevard du Triomphe, BE-1050 Bruxelles, Belgium

Abstract

We present a joint Molecular Dynamics (MD) / Kinetic Monte-Carlo (KMC) study aiming at the atomistic description of charge transport in stacks of liquid-crystalline tetra alkoxy-substituted metal-free phthalocyanines. The molecular dynamics simulations reproduce the major structural features of the mesophases, in particular a phase transition around 340 K between the rectangular and hexagonal phases. Charge transport simulations based on a Monte-Carlo algorithm show an increase by two orders of magnitude in the hole mobility when accounting for the rotational and translational dynamics. The results point to the formation of dynamical structural defects along the columns.

1. Introduction

Since their discovery at the end of the nineteenth century [1], liquid crystals (LC) have attracted a lot of fundamental interest and have been widely exploited at the technological level in liquid-crystal displays. These materials form self-organized assemblies over large areas up to the centimeter scale [2] with a different degree of orientational and positional order depending on the shape of the molecular backbone and the nature and the length of the side chains added to tune the physical properties [3,4,5]. Recently, liquid crystals have also been used in opto-electronic devices such as light-emitting diodes [6], solar cells [7], and field-effect transistors [8]. This is motivated by the possibility of modulating the nature of the side chains to achieve a LC character at room temperature [9,10] and hence avoid the formation of grain boundaries via self-healing properties, in contrast to crystalline materials. Discotic molecules made of a conjugated core surrounded by lateral saturated side chains are of particular interest due to their spontaneous self-organization into one-dimensional columns that creates efficient directional pathways for charge and exciton transport [11,12]. This is exemplified by hexabenzocoronene (HBC) derivatives that have been exploited in solar cells [7] and field-effect transistors [13].

Phthalocyanine (PC) derivatives represent another family of attractive planar conjugated molecules owing to their ease of synthesis. Numerous members of the PC family have been synthesized by varying the number, nature, length, and position of the flexible substituents as well as by incorporating a metal ion in the central cavity [14,15,16,17,18,19,20,21]. The main effects of chemical substitution is to tune both the thermotropic properties [12] and/or the electrical properties [22]. PC derivatives have been extensively used in organic solar cells due to the fact that the lowest absorption band (around 1.8 eV) overlaps in a very efficient way with the solar emission spectrum [23]; in addition; they exhibit a relatively low oxidation potential (6.41 eV from the gas-phase Ultraviolet Photoelectron spectrum of unsubstituted PC) [24] and are thus good candidates for electron donors in organic solar cells [25]. Moreover, they have been shown to form intercalated assemblies with perylene derivatives [26], an electron acceptor known for its high electron affinity and good charge transport properties [27]. This combination is thus expected to promote high performances in organic solar cells. Recently, with the help of surface

nanostructuration [28,29], it has also been demonstrated that PC could be aligned on large domains, which make them attractive for use in field-effect transistors.

This paper focuses on charge transport which is a key process governing the overall efficiency of most organic-based devices [30]. In the case of the alkoxy PC derivative considered in the following, different behaviors have been revealed by complementary experimental techniques. Hole mobility values around 0.2 cm^2/Vs are measured by the PR-TRMC (Pulse-Radiolysis Time-Resolved Microwave Conductivity) technique, which probes charge transport at a very local scale [31,32]. In contrast, Time-of-Flight measurements (TOF) yield hole mobility values on the order of only 10^{-3} cm^2/Vs (1×10^{-3} cm^2/Vs in the rectangular phase at 303K and 2.6×10^{-3} cm^2/Vs in the hexagonal phase at 373K) [33], thus suggesting that the structural defects encountered by the charges when drifting across the organic thin film strongly affect the charge transport properties, in agreement with previous experimental studies [34]. In order to develop discotic liquid crystals yielding maximized mobility values at the macroscopic scale, it is of prime importance to shed light into the charge transport properties at the molecular scale. This is a complex problem since the charge transfer rates are known to be highly sensitive to the relative positions of the units [11], which are further modulated by the lattice dynamics [35,36].

When compared to molecular crystals, liquid crystals display a static positional disorder introducing variations in the electronic couplings between the molecules as well as a static energetic disorder yielding a distribution of energies for the transport levels (i.e., the HOMO level of the individual molecules in the case of hole transport); these two types of disorder are further supplemented by a dynamic component induced by the thermal fluctuations [37]. The modeling of charge transport in disordered systems has been pioneered by the Monte-Carlo simulations of Bässler and co-workers assuming a hopping regime in which charges jump from molecule to molecule, with a rate dictated by effective parameters [38]. These simulations were performed in the early days on the basis of model lattices without accounting for the exact structural packing and the exact nature of the molecular compounds. This can be improved by propagating the charges in the hopping regime in structures provided by X-ray diffraction experiments or simulated with atomistic or coarse-grained techniques [39,40], and by estimating the transfer rates from quantum-

chemical calculations [41,42]. A joint classical/quantum-chemical (QCM) approach of this type has been recently applied to hexabenzocoronene stacks by propagating a charge in frozen one-dimensional columns with an explicit account of energetic disorder [43]; in these systems, the fluctuations of the transfers integrals induced by thermal disorder appear to slightly increase (by 25%) the mobility values.

In this work we wish to further extend this QCM approach by making full use of the molecular dynamics trajectory to this purpose we have first modeled by means of atomistic simulations the structural organization of liquid-crystalline PC derivatives substituted by four alkoxy chains, as recently synthesized by Geerts and co-workers [12] (see chemical structure in Figure 1). Starting from the simulated morphologies, we have calculated at the quantum-chemical level the electronic coupling between adjacent units along the dynamic trajectory; we have then estimated via Monte-Carlo simulations the hole mobility in the stacks considering both frozen geometries and an explicit account of the lattice dynamics. In the latter case, mobilities are found to be increased by two orders of magnitude, in contrast to the results obtained for HBC stacks [43]. The two different approaches allow us to reconcile the large disparity between the PR-TRMC and TOF mobility values reported for phthalocyanines. The paper is organized as follows: Section 2 focuses on the structural analysis of the molecular packings obtained by molecular dynamics simulations while section 3 describes the charge transfer parameters and charge carrier mobilities obtained for the rectangular and hexagonal mesophases of the PC derivative. Finally, conclusions and perspectives are given in section 4.

2. Structural Properties

2.1. Theoretical methodology

The individual molecules were described at the united atom, *i.e.* all hydrogen atoms were condensed with the closest heavy atoms, except for the two lying in the core. The new AMBER united atom force field parameters [44] were used for all atom types, with the exception of the aromatic carbons bearing a hydrogen, for which we used the parameters derived in [45]. The atoms forming the core, the oxygen atoms and the methylene units attached to them were endowed with atomic point charges, as

calculated from the electrostatic potential (ESP charges) [46] on the basis of the B3LYP/6-311G(d,p) optimized geometry of the C_s isomer of the tetra hydroxyl-substituted phthalocyanine using the Gaussian03 package [47]. Since each lateral chain contains a chiral centre and a racemic mixture is generally used in the experiments, we did not add in the force field the improper torsional term apt to retain the chirality for united atom centers [48].

Molecular Dynamics (MD) simulations were run in the NpT ensemble (p = 1 atm) with the NAnoscale Molecular Dynamics (NAMD) code [49] for simulation cells containing 80 molecules (10080 centers). We employed periodic boundary conditions (PBC), an orthorhombic box with a variable aspect ratio, and weakly coupled thermostat and barostat [50]. We adopted a time step of 1 fs for bonded interactions and of 4 fs for non-bonded interactions, respectively. The electrostatic long-range contributions were evaluated with the particle mesh Ewald algorithm [51] with a grid spacing of about 1.5 Å. The initial configuration consisted of four columns of 20 exactly superimposed molecules, arranged on a regular square lattice. A sample made of four columns is the minimal possible size to study hexagonal or rectangular packing; however, we ruled out the possibiliy of simulating eight columns of ten molecules since this choice could have reduced or biased the formation of structural defects along a single column and hence the realism of the simulations of the one-dimensional charge transport. The columns evolve into a hexagonal array after about 10 ns of equilibration at 450 K. Starting from this sample, we performed an equilibration run of about 50 ns before beginning a new run at a temperature of 25 K lower, repeating the scheme until T=300 K was reached. After equilibration, we find that columnar rectangular and columnar hexagonal phases are achieved at 300 K and 425 K, respectively, in full consistency with experimental thermotropic data [12]; the ensuing 65 ns-long production trajectories were used for the simulation of charge transport. Radial and tilt angle distributions have been analyzed in very large samples made of 1440 molecules obtained by replicating 8 times the equilibrated 80-molecule cells; two short simulations (one for each phase) of 3 ns were carried out with PBC, using only the last 2 ns of each trajectory for the calculation.

2.2. Results

The reliability and usefulness of a computer simulation is often measured in terms of its ability to reproduce experimental phase behavior and physical properties, and possibly in the ability of giving insights that are not easily accessible by experiments. In the literature, a few examples can be found where hexagonal or rectangular phases have been obtained for porphyrines, triphenylenes [39,52,53], and hexabenzocoronenes [54]; the level of agreement with experiment is variable but generally satisfying. In our case, the calculated densities of the samples (1.08, 1.01, 0.99 g/cm^3 at 300, 400, 425 K respectively) match quite well the experimental values inferred from X-ray diffraction (1.09-1.1, 1.00 g/cm^3 at 300 and 383 K, respectively [12,55]), thus providing a first validation of the force field. Even though an analysis of the full temperature dependence of the physical properties is beyond the scope of this paper, we stress that the system is still ordered at 450 K (the experimental clearing temperature is 500 K) and that the analysis of the temperature dependence of rotational and translational diffusion shows a columnar-columnar phase transition between 325 K and 350 K, *i.e.* very close to the experimental rectangular-hexagonal transition at 340 K.

In order to better characterize these two phases, we have calculated the radial distributions of the core hydrogens, see Figure 2. At both temperatures, the distributions are dominated at short distances (< 25 Å) by a sequence of peaks centered at multiples of the intermolecular stacking distance within a column. Their intensity is rapidly attenuated with increasing distance, in agreement with the short correlation length (around 3.7 nm) revealed by atomic force microscopy measurements on spin-coated phthalocyanines of similar nature [55]. At larger distances, broader peaks associated to intercolumnar separations appear at about 30 Å and its multiple at 60 Å; this is fully consistent with the X-ray values of **b** = 29.8 Å (at 300 K) for the rectangular phase and of **a** = 30.0 Å (at 383 K) for the hexagonal phase [12]. Such distances point to a strong interdigitation of the alkyl chains, as visualized for the seven molecules extracted from a typical snapshot of the hexagonal phase. A secondary peak is observed at about 50 Å and is associated to a separation between second nearest neighbor columns (green arrow in Figure 4). This peak should be centered at $\sqrt{3}\,\mathbf{a} \approx 52$ Å for the hexagonal phase and should shift towards slightly lower values in the rectangular phase (*i.e.* to the experimental cell parameter **a** = 46.7

Å at 300 K); however, it is hard to distinguish such a shift from the broad peaks in the radial distribution.

We have also characterized the rotational dynamics in the two phases on the basis of the time-autocorrelation function $\langle \vec{u}(0) \cdot \vec{u}(\tau) \rangle$ of the molecular axes, see Figure 3 with $\vec{u}$ denoting one of the three molecular axes (**x**, **y** and **z**)**;** these values have been averaged over the 80 molecules of the unit cell. The rotation of the **z** molecular axis, lying parallel to the columnar axis, is hindered at both temperatures, thus pointing to a much reduced off-plane motion. In contrast, two different regimes are found for the in-plane rotation described here by the **x** molecular axis: the rotation is relatively fast at high temperature (timescale of tens of nanoseconds) while it is severely hindered in the low temperature phase, as expected [15]*;* the Arrhenius plot in the inset of figure 3 confirms the presence of two regimes for the in-plane rotation as function of temperature. The rotational freezing at lower temperature is further confirmed by the distribution of the in-plane component of the intermolecular vector connecting the mass centers of two adjacent molecules belonging to the same column **r**=(Δx, Δy, Δz) (Figure 4); the latter does not show any preferred orientation at high temperature whereas it looses its isotropy at 300 K and exhibits a maximum along the (Δx, Δy=0) direction. Moreover, the configuration displaying two neighbor molecules with exactly superimposed mass centers (Δx=0,Δy=0, *i.e.*, with the intermolecular vector parallel to the columnar axis) becomes clearly disfavored at 300 K, thus yielding an overall tilt of the molecules with respect to the columnar axis, which is normally associated to rectangular phases. Plotting the distribution of the tilt angle ϕ between the **z** molecular axis and the columnar axis clearly reveals the existence of a non-tilted phase at 425 K and of a tilted phase at 300 K, as observed for the hexagonal and rectangular phases, respectively [56]. The average value of ϕ is approximately 15 degrees, in perfect agreement with experiment [55].

In summary, using a general united-atom force field, we have been able to obtain densities, rectangular-hexagonal phase transition temperature, cell parameters, and tilt angle in good agreement with experimental data. Since it has been shown for calamitic liquid crystals [4] that a force field reproducing transition temperatures and densities also provides reliable information for many other physical properties, we are

confident that the configurations obtained can be exploited for performing realistic charge transport simulations.

3. Charge transport properties

3.1. Theoretical methodology

We have modeled charge transport along the stacks in the hopping regime, as appropriated to the intrinsically disordered nature of liquid crystals. The rate of charge hopping between two adjacent molecules has been estimated in the framework of the Marcus-Levitch-Jortner (MLJ) formalism [57]:

$$k_{hop} = \frac{2\pi}{\hbar} t^2 \sqrt{\frac{1}{4\pi\lambda_S k_B T}} \sum_{n=0}^{\infty} \exp(-S) \frac{S^n}{n!} \exp\left[-\frac{(\Delta G^0 + \lambda_S + n\hbar\omega_i)^2}{4\lambda_S k_B T} \right] \quad (1)$$

with n going up to 50 to ensure the convergence of the k_{hop} *values,* T the temperature and k_B the Boltzmann constant. We note that Kumar et al. have shown that the introduction of two effective modes to describe the low and high-frequency motions is not expected to modify significantly the calculated rates [58].

- t is the transfer integral that reflects the strength of the electronic coupling between the HOMO orbitals of the two molecules involved in the hole transfer; this molecular parameter is highly sensitive to the relative position of the molecules and is strongly affected by changes in the intermolecular separations as well as by translational and rotational degrees of freedom [11,12,59]. We have computed the transfer integrals at the semi-empirical Hartree-Fock INDO (Intermediate Neglect of Differential Overlap) level by evaluating the direct coupling between the HOMOs of the two individual molecules [60] instead of relying on the energy-splitting-in-dimer method which is sometimes strongly biased by electronic polarization effects [61]. The choice of the INDO method is motivated by the fact that: (i) it generally yields a very good quantitative agreement when compared to results obtained with first-principle Hartree-Fock or DFT (Density Functional Theory) calculations [30]; (ii) it would have been prohibitive to compute at the *ab initio* level the transfer integrals for a large number of different dimers. In order to further reduce the computational efforts the PC alkyl chains have been replaced by hydrogen atoms in all calculations.

- S is the Huang-Rhys factor associated to a single effective intramolecular vibrational mode (with a typical energy ħω set here to 0.2 eV) that assists the charge transfer by allowing for tunneling across the energy barrier. S is directly related to the internal reorganization energy λ_i (= $S \cdot \hbar\omega$) that depicts the changes in the geometry of the two molecules during the electron transfer reaction $PC_1^+ + PC_2 \rightarrow PC_1 + PC_2^+$. λ_i has been estimated at the Density Functional Theory (DFT) level using the B3LYP functional and a 6-31G(d,p) basis set to be 114 meV for holes for the phthalocyanine derivative under study; this is a relatively low value, close to that of pentacene (95 meV) that displays one of the lowest λ_i among organic semiconductors [62]. The choice of this DFT approach is motivated by previous theoretical studies showing that it provides a very good quantitative agreement for several organic semiconductors when compared to experimental λ_i values deduced from gas-phase Ultraviolet Photoelectron Spectra (UPS) [62].

- λ_s is the external reorganization energy that accounts for the nuclear displacements in the surrounding medium and the resulting electronic effects [63]. This parameter cannot be easily accessed from quantum-chemical calculations, typical values range between 0.2 and 0.3 eV from simple models based on the dielectric properties of organic matrices [11]. We will set here λ_s equal to a value 0.2 eV; we stress that the main conclusions of this work would remain valid for the typical values of λ_s reported

- ΔG^0 is the Gibbs free energy associated to the electron transfer process. This represents, in a simple one-electron picture, the energy difference between the HOMO levels of the two interacting molecules. ΔG^0 is introduced in our simulations by the presence of an external electric field that promotes a preferential direction for charge transport by creating an energy gradient of the HOMO levels down the stacks:

$$\Delta G^0_{(ij)} = e \cdot \vec{F} \cdot \vec{d}_{(ij)} \qquad (2)$$

with $\vec{F}$ the electric field vector with a norm fixed to a typical value of 1000 V/cm and $\vec{d}$ the vector connecting the centroids of the electronic distribution associated to the HOMO level of the molecules i and j [41]. The transfer is favored when the hole moves along the direction of the applied electric field, which in our case coincides with the columnar axes orientation. Note that we have neglected here the impact of static and dynamic energetic disorder that also contributes to the ΔG^0 parameter since the primary focus of the present study is to investigate the influence of the dynamic

positional disorder on charge transport and not to provide absolute values of the charge mobilities.

The calculated transfer rates have then been injected into a Kinetic Monte-Carlo (KMC) algorithm in order to propagate a charge in the system and estimate the hole mobility. In our KMC scheme, detailed in [41], the charge is initially localized on a given molecule *i* and hops to the molecule *j*, chosen on the basis of the transfer probability expressed as:

$$p_{ij} = \frac{k_{ij}}{\sum_{l} k_{il}} \tag{3}$$

where k_{ij} is the transfer rate (corresponding to the inverse of the hopping time) between molecule *i* and *j* calculated with equation (1) and the sum index *l* runs over all possible neighbors of molecule *i.* After *n* hopping events, the mobility is calculated as:

$$\mu_n = \frac{d_n}{t_n \cdot F} \tag{4}$$

with d_n is the total distance traveled by the charge in the field direction during the simulation time t_n and *F* the norm of the electric field. A large number of hopping events (more than 10^{10} iterations) have been generated in order to get converged estimates of the mobility values, as supported by the standard deviation values [41].

3.2. Results

3.2.1. Transfer integrals

We have calculated the transfer integrals and have analyzed them in parallel with the geometric configurations of the PC dimers along the stacks. This has been done on the basis of 650 configurations separated by 100 ps that were extracted from a MD run. The large number of configurations ensures the statistical reliability of the analysis; the large lapse of time between the snapshots has been chosen in order to minimize time correlation between the geometric variables. Each dimer has been geometrically characterized by six coordinates: three associated to translations (Δx,

Δy, and Δz that describe the relative position of the centers of mass of the two molecules according to their atomic Cartesian coordinates) and three to rotations (characterized by the Euler angles α, β, and γ that define the relative rotational orientation of the two molecules using the **z-x-z** convention, with **z** aligned along the columns axis and **x** along the intercolumns direction). In both phases, the transfer integrals are negligible between molecules located in adjacent columns so that charge transport is strictly one-dimensional and occurs between nearest neighbors within a column. Significant translational and rotational motions of the PC cores occur during the molecular dynamics trajectory and strongly impact the transfer integral values. Unexpectedly, the different structural properties of the two mesophases lead to similar distributions and similar average transfer integral values (60 and 58 meV for the rectangular and hexagonal mesophases, respectively). This is evidenced in Figure 5 showing a broad distribution of transfer integrals in the two phases when collecting the values for the 650 snapshots. Plotting the distributions in a log-log scale clearly shows a tail associated with geometric configurations promoting very small transfer integrals, which may act as traps.

We start the analysis of dimer configurations by showing in Figure 6 the two-dimensional plots of the probability of (β,Δz) at 300 K and 425 K. The two plots reveal β values ranging from 0 to 20 degrees and an increase in the Δz spacing from 3.2 to 3.8 Å between these two limits. The increase in Δz with β is rationalized by the fact that introducing a tilt between the two molecular planes would induce a strong steric repulsion in one part of the dimer if Δz is kept constant. The most probable values lie in between 2 and 12 degrees for β and in between 3.5 and 3.7 Å for Δz. The distributions of transfer integrals as well as the average transfer integrals value obtained for different ranges of β angles (from 0 to 5, 5 to 10, 10 to 15, and 15 to 20 degrees) are found to be similar (see Figure 7a). This can be rationalized from Figure 7b showing the evolution of the transfer integrals in a model system made of two exactly superimposed PC molecules (with intermolecular distances of 3.54 and 3.60 Å representative of the distributions) when varying the β angle from 0 degree (cofacial configuration) to 25 degrees. In both cases, the transfer integral increases with a growing β angle due to the strong contacts promoted between the two molecules on one side of the dimer; this effect is not compensated by the looser contacts created on the other side in view of the exponential dependence of the transfer integral as a

function of the intermolecular distance [12]. When reporting in Figure 7b the most probable β angle in the rectangular phase for the two chosen Δz values (7 and 10 degrees for 3.54 and 3.60 Å, respectively), we do obtain similar transfer integrals, as explained by the concomitant increase in the intermolecular separation that accompanies an increase in the β angle; the same conclusions hold true for the hexagonal phase. It is worth noting that the transfer integral values calculated for this model system are larger by one order of magnitude compared to the average value in the actual stacks, thus pointing to the key role played by positional disorder [37].

Since the β values are relatively small in all dimers, α and γ are nearly degenerate. It is thus convenient to follow the distribution of θ = α + γ, which is representative of the relative in-plane rotation of the molecules. The distribution of θ in the interval 0-180 degrees shows in both phases a broad peak lying between 60 and 120 degrees, with a maximum around 90 degrees. The latter situation hinders the inner hydrogens of the PC cores to superimpose. This indicates that the PC molecules stay preferentially in an eclipsed conformation in order to maximize the attractive van der Waals interactions between the saturated chains (Figure 8a). Interestingly this feature has been also predicted by DFT-D calculations for porphine dimer [64]; a molecule which present a similar core to PC. The evolution of the calculated average transfer integral as a function of the rotational orientation of the PC cores exhibit a very different behavior in the rectangular *versus* hexagonal mesophases. $\langle t \rangle$ appears to be almost independent of the orientation θ of the molecules within the dimer at 425K whereas it oscillates at 300K with maximum (minimum) values around n times π/4 (π/8 + n π/4), with n an integer number (Figure 8b). Such fluctuations are also found when rotating one PC molecule with respect to the other in a perfectly cofacial geometry (Figure 8c); note that zero values are associated to geometries yielding a complete cancellation of the bonding *versus* antibonding interactions in the overlap region [65]. The lower magnitude of the transfer integrals calculated in the mesophases and the peculiar behavior observed in Figure 8a points to the key additional role played by the translational degrees of freedom. The significant differences observed in Figure 8b between the two phases contrast with the very similar distribution of transfer integrals reported in Figure 5; this is rationalized by variations in the degree of translations between the two phases, as illustrated in

Figures 9a and 9b by plotting the (Δy,Δx) probability for both mesophases at θ=70 degrees. In the rectangular phase (Figure 9a), the molecules show a preferential displacement along the **x** direction, with shifts from the perfectly cofacial configuration, which bring the largest contributions to the transfer integrals (see Figure 9c) by a distance lying between 1 and 2.5 Å, with a maximum around 1.5 Å. In the hexagonal phase, the 2D map is quite isotropic and gives a non-zero probability for the cofacial configuration (Δx=0,Δy=0) in contrast to the tilted rectangular phases. A similar analysis can be done for other θ angle values and the same conclusions can hold. The results thus further indicate that the molecules are much more constrained in the rectangular phase compared to the hexagonal phase.

3.2.2. Charge Mobility

The role of static *versus* dynamic disorder in chemical systems has to be properly assessed in order to depict charge transport in organic semiconductors. On one hand, amorphous materials such as polymer thin films have been successfully described on the basis of a static disorder characterized by a Gaussian distribution of site energies and transfer integrals [38]. On the other hand, the experimental temperature dependence of the mobility in organic molecular crystals is best reproduced when accounting for a loss of coherent transport at high temperature due to thermal fluctuations of the transfer integrals and site energies [66,67]. For the disordered liquid crystalline phases under study, a central question is to know whether the system should be treated as fully static or if a dynamic contribution should be taken into account. In order to address this issue, we have plotted in Figure 10 the time autocorrelation function of the absolute value of the transfer integral (averaged over the 80 molecules of the cell). A multiexponential decay of the autocorrelation function occurs in the nanosecond time scale, but it is much slower in the rectangular phase (~50 ns) than in the hexagonal phase (~3 ns), consistently with the rotational auto-correlation functions shown in Figure 3. Charge transport thus appears to be more correlated at 300 K. However, fast local fluctuations of the transfer integrals are observed during the timescale of a charge transfer event (on the order of the picosecond) and are likely to impact the charge migration along the columns. These are singled out in the inset of Figure 10, which shows the short time behavior of the

correlation function as calculated from a MD trajectory lasting 20 ps with snapshots extracted every 10 fs.

The fast fluctuations of the electronic coupling are further evidenced in Figure 11 showing the evolution over 5 ps of the transfer rate from a given molecule to the nearest neighbors (*i.e.*, in a direction parallel and opposite to the electric field) in the rectangular phase. Interestingly, situations where the charge transfer probability is negligible or where the charge transfer in the direction opposite to the electric field is more favorable do happen regularly and are not attenuated by the presence of high electric fields (up to 10^6 V/cm). In these instances, the charge is thus blocked for a finite time over a part of the column that acts as a defect of dynamic nature. Such a defect is temporarily created by specific translations and/or rotations yielding a geometry characterized by a very small transfer integral along the electric field direction.

In order to get a deeper insight into the influence of such dynamical defects on the transport properties, we have calculated the charge mobility along the stacks in two different ways, namely in a purely static limit and with an approach taking into account lattice dynamics. In the static picture, we have propagated via Monte-Carlo simulations a hole in each configuration extracted from the MD simulation and have calculated the average hole mobility over 650 snapshots separated by 100 ps; in this case, since the molecules are frozen during the KMC evolution, the lifetime of a defect is infinite. Doing so, we obtain similarly low mobility values of 3.12×10^{-3} and 2.92×10^{-3} cm²/Vs in the rectangular and hexagonal mesophases, respectively. Interestingly, the calculated mobility has the same order of magnitude as the value provided by TOF measurements ($\mu=10^{-3}$ cm²/Vs [33]) for a very similar PC derivative; this is consistent with the fact that the TOF mobility values are known to be limited by the presence of static defects. In the dynamic approach, in view of the fast thermal fluctuations, we have performed Monte-Carlo simulations based on hopping rates averaged for each dimer over the 650 snapshots of the whole dynamics of 65 ns; such an averaging of the transfer integral is typically achieved when considering that the system explores a large conformational space before the charge transfer occurs [36]. In this approach, the system is defect free and the transfer rate in the forward direction (*i.e.*, parallel to the electric field) is always larger than in the backward direction. The mobility is only limited here by the hopping events in the

direction opposite to the electric field. In this framework, the hole mobility is estimated to be two orders of magnitude larger (around 0.1 cm²/Vs) at both temperatures. Interestingly, this value is very close to that given by the PR-TRMC technique (μ=0.08-0.37 cm²/Vs [31]) which probes the transport at the nanoscale in defect-free regions.

The huge difference between the mobilities provided by the two approaches suggests the presence of many dynamic structural defects along the columns. This has been quantified by spotting every single defect in the 650 configurations of the system and by classifying them according to the transfer probability $p_{\rightarrow}$ to cross the defect (namely, the ratio of the transfer rate along the electric field direction over the sum of the forward and backward transfer rates). Defects characterized by $p_{\rightarrow}$ lower than 10 percents, which are likely to influence the most charge transport, are by far the most numerous (see Table 1). We have also calculated the time required to cross the defect; since the distance between the molecules is always approximately the same (3.6 Å), this parameter directly reflects the impact of molecular misalignment on the charge mobility. In practice, we position the charge initially in front of a defect and perform a KMC simulation to make it cross the defect. The crossing time is then averaged over all defects collected in the 650 configurations and compared to the corresponding average time in absence of defects (*i.e.*, for situations with a transfer probability larger than 50 percents), see Table 2. The results reveal that the transit time is reduced by two orders of magnitude in presence of defects with the lowest transfer probability ($p_{\rightarrow}$ = 10 percents), thus demonstrating that the static mobility values are predominantly limited by the presence of such defects. We stress that the impact of static defects is amplified in phthalocyanine derivatives due to the one-dimensional character of charge transport; indeed, there is no other solution than to keep propagating the charge along a given column, in comparison with two or three-dimensional transport encountered in molecular crystals. The present results contrast with recent theoretical data reported for hexabenzocorone stacks [43] pointing to a slight increase (by 25%) of the mobility values when taking into account the lattice dynamics. This might be attributed to the fact that the HBC molecule has a doubly degenerate HOMO level in contrast to PC; there are thus in HBC stacks two independent conducting pathways for charge hopping between two adjacent molecules that generally act in a complementary way [12]; this implies that when the

conduction channel is closed via one electronic channel, the charge transfer is very often favored by the other, thus making the system much less sensitive to positional defects.

4. Conclusions

In this paper, we have combined Molecular Dynamics simulations with a Kinetic Monte-Carlo approach in order to estimate the hole mobility values in columnar mesophases made of tetra alkoxy-substituted phthalocyanine derivatives. The molecular packing simulated by means of the MD approach reproduces the structural characteristics found experimentally for the low-temperature columnar rectangular and high-temperature columnar hexagonal phases. The analysis reveals that the rectangular phase exhibits a tilt angle of 15° which prevents PC molecules to lie in the fully cofacial configuration which maximizes transfer integral values. However, the two mesophases exhibit a very similar distribution of transfer integrals due to their different degree of rotational and translational motions as well to their different dynamic of molecular motions. The hole mobility values were then computed via a Kinetic Monte-Carlo algorithm bases on transfer rates provided by the Marcus-Levich-Jortner formalism, with the main molecular parameters evaluated at a quantum-chemical level. The charge carrier mobility in the phthalocyanine stacks has been estimated with two different approaches that are expected to provide a lower and upper bound for this parameter. The static approach averages the mobility over 650 frozen configurations of the system and leads to a value of 10^{-3} cm²/Vs. The dynamic approach relies on transfer rates averaged over 650 snapshots of the MD run and yields mobility value of 10^{-1} cm²/Vs. The increase by two orders of magnitude going from the static to the dynamic picture is explained by the presence of dynamic defects in the latter case which get self-repaired with time due to thermal motion. These results further reconcile the large disparity between the mobility values provided by TOF *versus* PR-TRMC measurements. The role of lattice dynamics appears to be more pronounced here than in a previous study performed on hexabenzocoronene stacks, as probably due to the absence of degeneracy of the HOMO levels in PC.

Acknowledgements

The research leading to these results has received funding from the European projects MODECOM (NMP3-CT-2006-016434), NAIMO (NMP4-CT-2004-500355) and ONE-P (NMP3-LA-2008-212311). The work in Mons has been partly supported by the Marshall plan of the Walloon Region, in the framework of project MIRAGE (MIse au point de Revêtements de surface Actifs pour une meilleure Gestion de l'Environnement). The work in Mons is further supported by the Belgian National Fund for Scientific Research (FNRS). J.C. is an FNRS Research Fellow.

References

[1] Collings, P. J.; Hird, M.; *Introduction to Liquid Crystals Chemistry and Physics*, Taylor & Francis, London and New-York (1997).

[2] Tracz, A.; Makowski, T.; Masirek, S.; Pisula, W.; Geerts, Y. H. *Nanotech.* **2007**, *18*, 485303.

[3] Sergeyev, S.; Pisula, W.; Geerts, Y. H. *Chem. Soc. Rev.* **2007**, *36*, 1902.

[4] Tiberio, G.; Muccioli, L.; Berardi, R.; Zannoni, C. *ChemPhysChem* **2009**, *10*, 125.

[5] Seguy, I.; Jolinat, P.; Destruel, P.; Farenc, J.; Mamy, R.; Bock, H.; Ip, J.; Nguyen, T. P. *J. Appl. Phys* **2001**, *89*, 5442.

[6] Feng, X., Marcon, V.; Pisula, W.; Hansen, M. R.; Kirkpatrick, J.; Grozema, F.; Andrienko, D.; Kremer, K.; Müllen, K. *Nature Mater.* **2009**, *8*, 421.

[7] Schmidt-Mende, L.; Fechtenkotter, A.; Müllen, K.; Moons, E.; Friend, R. H.; MacKenzie, J. D. *Science* **2001**, *293*, 1119.

[8] Bunk, O.; Nielsen, M. M.; Solling, T. I.; van de Craats, A. M.; Stutzmann, N. *J. Am. Chem. Soc.* **2003**, *125*, 2252.

[9] Liu, C. Y.; Fechtenkötter, A.; Watson, M. D.; Müllen, K. and Bard, A. J. *Chem. Mater.* **2003**, *15*, 124.

[10] Sergeyev, S.; Debever, O.; Pouzet, E.; Geerts, Y. H. *J. Mater. Chem.* **2007**, *17*, 3002.

[11] Lemaur, V.; da Silva Filho, D. A.; Coropceanu, V.; Lehmann, M.; Geerts, Y. H.; Piris, J.; Debije, M. G.; van de Craats, A. M.; Senthilkumar, K.; Siebbeles, L. D. A.; Warman, J. M.; Brédas, J. L.; Cornil, J. *J. Am. Chem Soc.* **2004**, *126*, 3271.

[12] Tant, J.; Geerts, Y. H.; Lehmann, M.; De Cupere, V.; Zucchi, G.; Laursen, B. W.; Bjørnholm, T.; Lemaur, V.; Marcq, V.; Burquel, A.; Hennebicq, E.; Gardebien, F.; Viville, P.; Beljonne, D.; Lazzaroni, R.; Cornil, J. *J. Phys. Chem. B* **2005**, *109*, 20315. Additions and corrections : *J. Phys. Chem. B* **2006**, 110, 3449.

[13] van de Craats, A. M.; Stutzmann, N.; Bunk, O.; Nielsen, M. M.; Watson, M.; Müllen, K.; Chancy, H. D.; Sirringhaus, H.; Friend, R. H. *Adv Mat.* **2003**, *15*, 495.

[14] Guillon, D.; Skoulios, A.; Piechocki, C.; Simon, J.; Weber, P. *Mol. Cryst. Liq. Cryst.* **1983**, *100*, 275.

[15] van der Pol, J. F.; Neeleman, E.; Zwikker, J. W.; Nolte, R. J. M.; Drenth, W.; Aerts, J.; Visser, R.; Picken, S. J. *Liq. Cryst.* **1989**, *6*, 577.

[16] Engel, M. K.; Bassoul, P.; Bosio, L.; Lehmann, H.; Hanack, M.; Simon, J. *Liq. Cryst.* **1993**, *15*, 709.

[17] Van Nostrum, C. F.; Bosman, A. W.; Gelinck, G. H.; Schouten, P. G.; Warman, J. M.; Ketgens, A. P. M.; Devillers, M. A. C.; Meijerink, A.; Picken, S. J.; Sohling, U.; Schouten, A. J.; Nolte, R. J. M. *Chem. Eur. J.* **1995**, *1*, 171.

[18] Kroon, J. M.; Koehorst, R. B. M.; Van Dijk, M.; Sanders, G. M.; Sudhölter, E. J. R. *J. Mater. Chem.* **1997**, *7*, 615.

[19] Clarkson, G. J.; Cook, A.; McKeown, N. R.; Treacher, K. E.; Ali-Adib, Z.; *Macromolecules* **1996**, *29*, 913.

[20] Hatsusaka, K.; Ohta, K.; Yamamoto, I.; Shirai, H. *J. Mater. Chem.* **2001**, *11*, 423

[21] Norton, J. E.; Brédas, J. L. *J. Chem. Phys.* **2008**, *128*, 34701.

[22] Sergeyev, S.; Pouzet, E.; Debever, O.; Levin, J.; Gierschner, J.; Cornil, J.; Aspe, R. G.; Geerts, Y. H. *J. Mater. Chem.* **2007**, *17*, 1777.

[23] Edwards, L.; Gouterman, M. *J. Mol. Spectrosc.* **1979**, *33*, 292.

[24] Pullman, A.; Berthier, G. *C. R. Acad. Sci. (Paris)* **1953**, *236*, 1494.

[25] Orti, E.; Brédas, J. L.; Clarisse, C. *J. Chem. Phys.* **1990**, *92*, 1228.

[26] Zucchi, G.; Viville, P.; Donnio, B.; Vlad, A.; Melinte, S.; Mondeshki, M.; Graf, R.; Spiess, H. W.; Geerts, Y. H.; Lazzaroni, R. *J. Phys. Chem B* **2009**, *113*, 5448.

[27] Karl, N. *Synth. Met.* **2003**, *133*, 649.

[28] Mouthuy, P. O.; Melinte, S.; Geerts, Y. H.; Jonas, A. *Nano Lett.* **2007**, *7*, 2627.

[29] Mouthuy, P. O.; Melinte, S.; Geerts, Y. H.; Nysten, B.; Jonas, A. *Small* **2008**, *4*, 728.

[30] Coropceanu, V.; Cornil, J.; da Silva Filho, D. A.; Olivier, Y.; Silbey, R.; Brédas, J. L. *Chem. Rev.* **2007**, *107*, 926.

[31] van de Craats, A. M.; Schouten, P. G.; Warman, J. M. *J. Jap. Liq. Cryst. Soc.* **1997**, *2*, 12.

[32] Warman, J. M.; de Haas, M. P.; Dicker, G.; Grozema, F. C.; Piris, J. and Debije, M. G. *Chem. Mater.* **2004**, *16*, 4600.

[33] Deibel, C.; Janssen, D.; Heremans, P.; De Cupere, V.; Geerts, Y.; Benkhedir, M. L.; Adriaenssens, G. J. *Org. Electronics* **2006**, *7*, 495.

[34] Dimitrakopoulos, C. D.; Mascaro, D. J. *IBM J. Res. & Dev.* **2001**, *45*, 11.

[35] Troisi, A.; Orlandi, G.; *J. Phys. Chem. A* **2006**, *110*, 4065.

[36] Troisi, A.; Cheung, D. L.; Andrienko, D. *Phys. Rev. Lett.* **2009**, *102*, 116602.

[37] Palenberg, M. A.; Silbey, R. J.; Malagoli, M.; Brédas, J. L. *J. Chem. Phys.* **2000** *112*, 1541.

[38] Bässler, H. *Phys. Stat. Sol. (b)* **1993**, *175*, 15-56.

[39] Muccioli, L.; Berardi, R.; Orlandi, S.; Ricci, M.; Zannoni, C. *Theor. Chem. Acc*. **2007**, *117*, 1085.

[40] Orlandi, S.; Muccioli, L.; Ricci, M.; Berardi, R.; Zannoni, C. *Chem. Central J.* **2007** *1*, 15.

[41] Olivier, Y.; Lemaur, V.; Cornil, J.; Brédas, J. L. *J. Phys. Chem. A* **2006**, *110*, 6356.

[42] Kirkpatrick, J.; Marcon, V.; Nelson, J.; Kremer, K.; Andrienko, D. *Phys. Rev. Lett.* **2007**, *98*, 227402.

[43] Kirkpatrick, J.; Marcon, V.; Kremer, K.; Nelson, J. and Andrienko, D. *J. Chem. Phys.* **2008**, *129*, 094506.

[44] Yang, L. J.; Tan, C. H.; Hsieh, M. J.; Wang, J. M.; Duan, Y.; Cieplak, P.; Caldwell, J.; Kollman, P. A.; Luo, R. *J. Phys. Chem. B* **2006**, *110*, 13166.

[45] von Lilienfeld, O. A.; Andrienko, D. *J. Chem. Phys.* **2006**, *124*, 054307.

[46] Besler, B. H.; Merz Jr., K. M.; Kollman, P. A. *J. Comput. Chem.* **1990**, *11*, 431.

[47] Frisch M. J. et al. Gaussian 03, Revision C.02. Gaussian, Inc., Wallingford, CT, **2004**.

[48] Weiner, S. J.; Kollman, P. A.; Case, D. A.; Singh, U. C.; Ghio, C.; Alagona, G.; Profeta, S. Jr.; Weiner, P. *J. Am. Chem. Soc.* **1984**, *106*, 765.

[49] Phillips, J. C.; Braun, R.; Wang, W.; Gumbart, J.; Tajkhorshid, E.; Villa, E.; Chipot, C.; Skeel, R. D.; Kale, L. and Schulten K. *J. Comp. Chem.* **2005**, *26***,** 1781.

[50] Berendsen, H. J. C.; Postma, J. P. M.; van Gunsteren, W. F.; Di Nola, A.; Haak, J. R. *J. Chem. Phys.* **1984**, *81*, 3684.

[51] York, D. M.; Darden, T. A. and Pedersen, L. G. *J. Chem. Phys*. **1993**, *98*, 8345.

[52] Cinacchi, G.; Colle, R.; Tani, A. *J. Phys. Chem. B* **2004**, *23*, 7969.

[53] Cinacchi, G.; Colle, R.; Parruccini, P.; Tani, A. *J. Chem. Phys.* **2008**, *17*, 174708.

[54] Marcon, V.; Vehoff, T.; Kirkpatrick, J.; Jeong, C.; Yoon, D. Y.; Kremer, K.; Andrienko, D. *J. Chem. Phys.* **2008**, *129*, 094505.

[55] Gearba, R. I.; Bondar, A. I.; Goderis, B.; Bras, W.; Ivanov, D. A. *Chem. Mater* **2005**, *17*, 2825.

[56] Ghose, D.; Bose, T. R.; Saha, J.; Mukherjee, C. D.; Roy, M. K.; Saha, M. *Mol. Cryst. Liq. Cryst.* **1995**, *264*, 165.

[57] Jortner, J. *J. Chem. Phys.* **1976**, *64*, 4860.

[58] Kumar, K.; Kurnikov, I. V.; Beratan, D.; Waldeck, D. H.; Zimmt, M. B. *J. Phys. Chem. A* **1998**, *102*, 5529.

[59] Senthilkumar, K.; Grozema, F. C.; Bickelhaupt, F. M.; Siebbeles, L. D. A. *J. Chem. Phys.* **2003**, *119*, 9809.

[60] Van Vooren, A.; Lemaur, V.; Ye, A.; Beljonne, D. and Cornil, J. *ChemPhysChem* **2007**, *8*, 1240.

[61] Valeev, E. F.; Coropceanu, V.; da Silva, D. A.; Salman, S.; Bredas, J. L. *J. Am. Chem. Soc.* **2006**, *128*, 9882.

[62] Coropceanu, V.; Malagoli, M.; de Silva Filho, D. A.; Gruhn, N. E.; Bill, T. G. and Brédas, J. L. *Phys. Rev. Lett*. **2002**, *89*, 275503.

[63] Marcus, R. A. *J. Chem. Phys.* **1965**, *43*, 679.

[64] Mück-Lichtenfeld, C.; Grimme, S. *Mol. Phys.* **2007**, *105*, 2793.

[65] Brédas, J. L.; Calbert, J. P.; da Silva Filho, D. A.; Cornil, J. *Proc. Nat. Acad. Sci. USA* **2002**, *99*, 5804.

[66] Podzorov, V.; Menard, E.; Rogers, J. A.; Gershenson, M. E. *Phys. Rev. Lett.* **2005**, *95*, 226601.

[67] Troisi, A. *Adv. Mat.* **2007**, *19*, 2000.

	Percentage of defects	
Probability	**300K**	**425K**
0-10 %	23.0	22.4
10-20 %	8.8	8.9
20-30 %	6.8	6.8
30-40 %	5.9	6.1
40-50 %	5.4	5.6

Table 1: Percentage of defects as a function of the transfer probability along the electric field direction in the rectangular and hexagonal phases, calculated for a field F =1000 V/cm.

	Time to Cross a Defect (s)	
Probability	**300K**	**425K**
0-10 %	$1.94 \cdot 10^{-11}$	$1.49 \cdot 10^{-11}$
10-20 %	$1.93 \cdot 10^{-12}$	$1.41 \cdot 10^{-12}$
20-30 %	$1.08 \cdot 10^{-12}$	$7.88 \cdot 10^{-13}$
30-40 %	$6.91 \cdot 10^{-13}$	$4.96 \cdot 10^{-13}$
40-50 %	$4.90 \cdot 10^{-13}$	$3.58 \cdot 10^{-13}$
> 50%	$1.09 \cdot 10^{-13}$	$8.11 \cdot 10^{-14}$

Table 2: Average time to cross a defect (in seconds) cm in the rectangular and hexagonal phases, as a function of the transfer probability along the electric field F =1000 V/cm .

Figure captions

Figure 1: Schematic representation of a rectangular (i) and hexagonal (ii) mesophase. We also show (iii) the chemical structure of the tetra alkoxy-substituted phthalocyanine molecules under study featuring branched C_{12}-C_8 side chains.

Figure 2: Radial distribution of the core hydrogens in the rectangular (blue curve) and hexagonal (red curve) phases, with explicit assignment of the main peaks. In the inset, a snapshot of seven molecules belonging to different columns evidences the hexagonal packing and the interdigitation of alkyl chains

Figure 3: Autocorrelation function of the molecular axes **x** and **z** in the rectangular (empty symbols) and hexagonal (filled symbols) phases. In the inset, an Arrhenius plot at all simulated temperatures of the rotational time τ_1 about the x axis shows the presence of two different regimes, corresponding to hexagonal (high temperature, thin dashed line) and rectangular (low temperature, thick dashed line) phases. The lines represent fits of τ_1 with the equation $\tau_1(T)= \tau_0*\exp(-E_A/kT)$ for $T>325$ K and $T\leq 325$ K respectively. In-plane rotational times τ_1 were obtained at all simulated temperatures by fitting in the range 0-40 ns the autocorrelation functions of the main plot with triexponential functions and integrating them from t=0 to $t=\infty$.

Figure 4: (Left) Two-dimensional probability maps of the horizontal displacements of the interneighbor vector ($\Delta x,\Delta y$) in the rectangular (top) and hexagonal (bottom) phases. (Right) Distribution of the tilt angle ϕ in the rectangular and hexagonal phases; to confirm the presence of the tilt simulated columns in the two phases are shown as inset. Alkyl chains are not visualized.

Figure 5: Distribution of the transfer integrals between nearest neighbors calculated from the 650 snapshots of the molecular dynamics trajectory separated by 100 ps, for the rectangular (300K, blue line) and hexagonal phases (425K, red line).

Figure 6: Distribution of the angle between neighbor z axes β *versus* the vertical displacement Δz at **a)** 300 K and **b)** 425 K. The color index gives the probability to find a β value for a given Δz.

Figure 7: a) Distribution of transfer integrals obtained for different ranges of β angles (from 0 to 5, 5 to 10, 10 to 15, and 15 to 20 degrees). **b)** Evolution of the transfer integral of model cofacial dimer ($\alpha=\gamma=0$ degrees, $\Delta x=\Delta y=0$) as a function of the β angle for $\Delta z=3.54$ Å (red) and 3.60 Å (black), the dotted lines refer to the β value taken from the β *versus* the vertical displacement Δz in the rectangular phase.

Figure 8: a) Probability distribution of the rotational angle $\theta=\alpha+\gamma$ at 300 K and 425 K. Evolution of **b)** the ensemble-averaged transfer integral and **c)** the transfer integral in a model cofacial dimer as a function of the rotational angle θ.

Figure 9: Two-dimensional probability maps of the horizontal displacements of the interneighbor vector ($\Delta x,\Delta y$) in the **a)** rectangular and **b)** hexagonal phases for a rotational angle θ of 70 degrees. Two-dimensional maps of the transfer integral as a function of the interneighbor vector ($\Delta x,\Delta y$) in a model system of PCs for $\beta=0$.

Figure 10: Time autocorrelation functions of the transfer integral for a MD simulation of 65 ns with a time spacing between the configurations of 100 ps. The inset shows the equivalent functions for a MD run of 20 ps with a time spacing between the configurations of 10 fs.

Figure 11: Time evolution of the transfer rate along the electric field direction ($d>0$, red curve) and in the direction opposite to the field ($d<0$, green curve) in a trimer of PC molecules extracted from a column. The orange (blue) circle represents a situation where charge transfer is more likely to occur along the electric field direction (in the direction opposite to the electric field). The inset shows the corresponding time evolution of the transfer integrals.

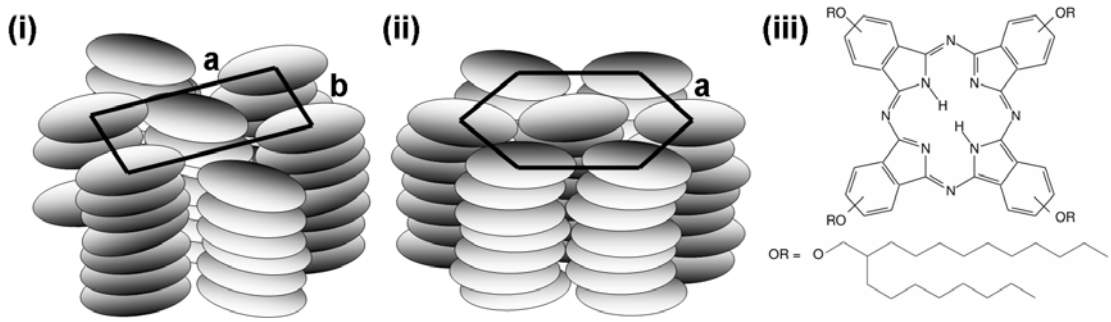

Figure 1 Olivier et al.

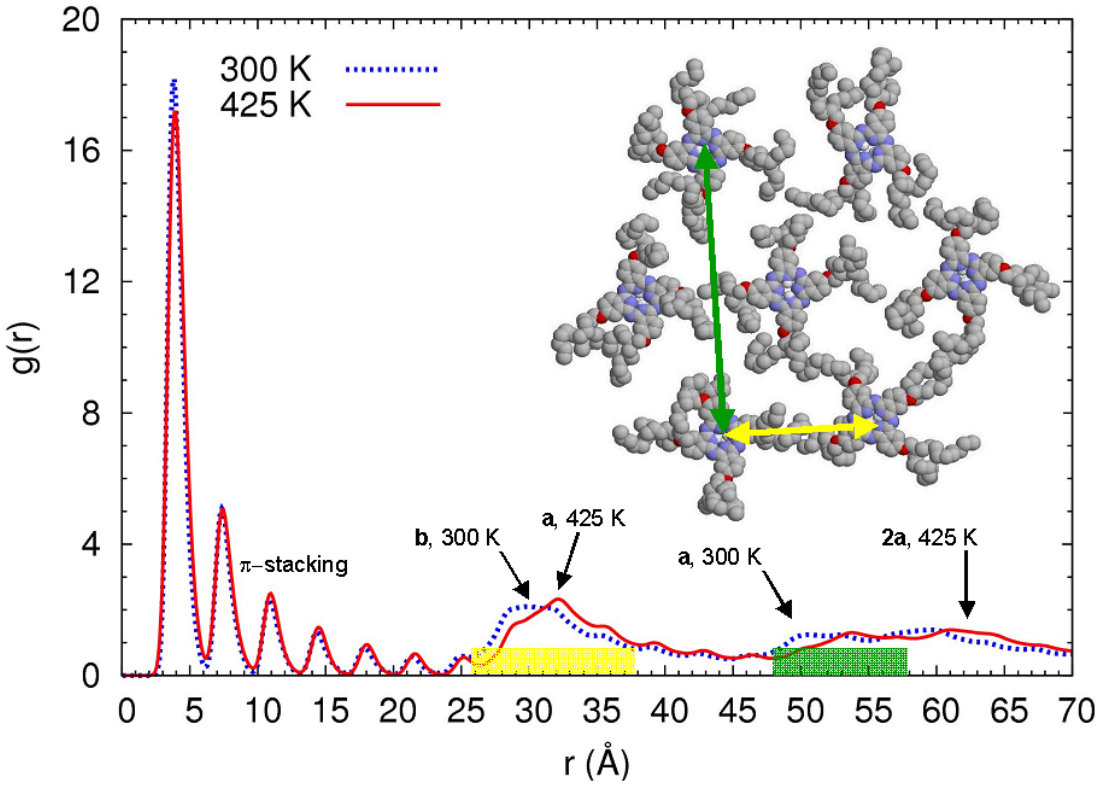

Figure 2 Olivier et al.

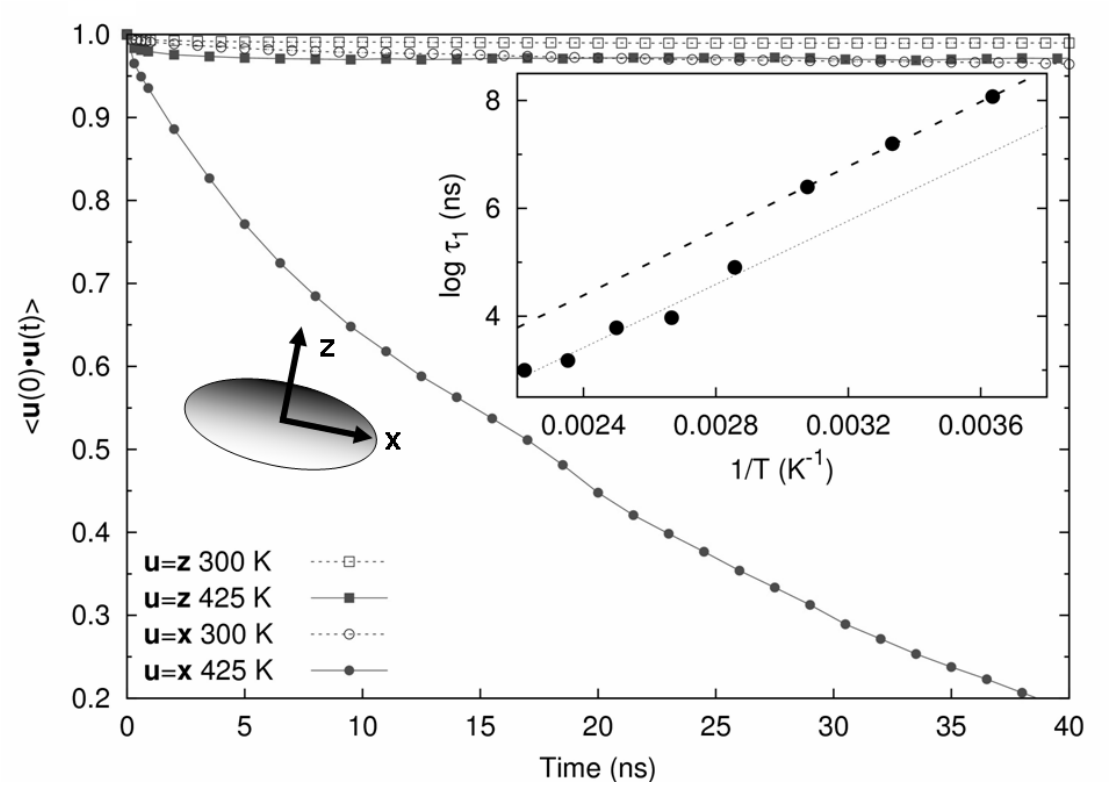

Figure 3 Olivier et al.

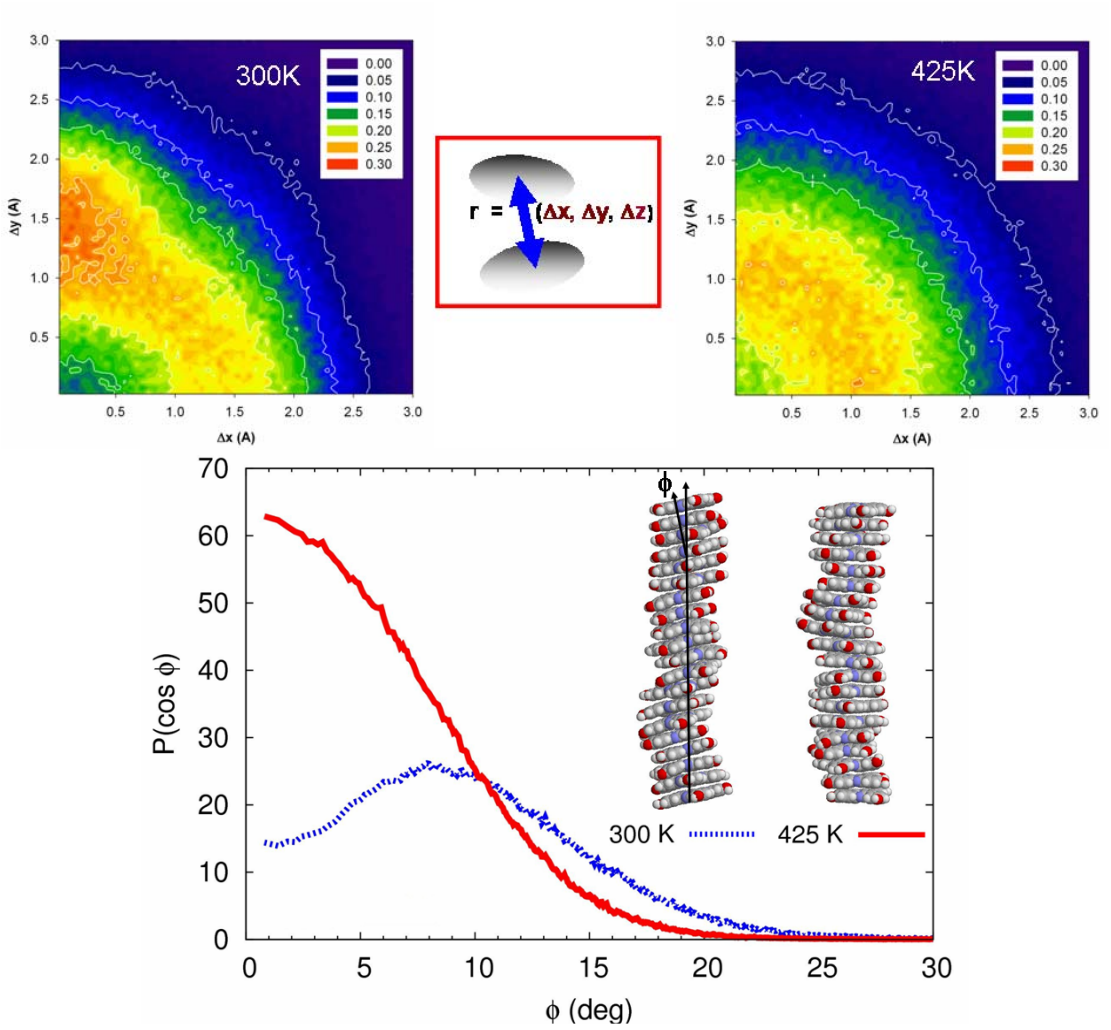

Figure 4 Olivier et al.

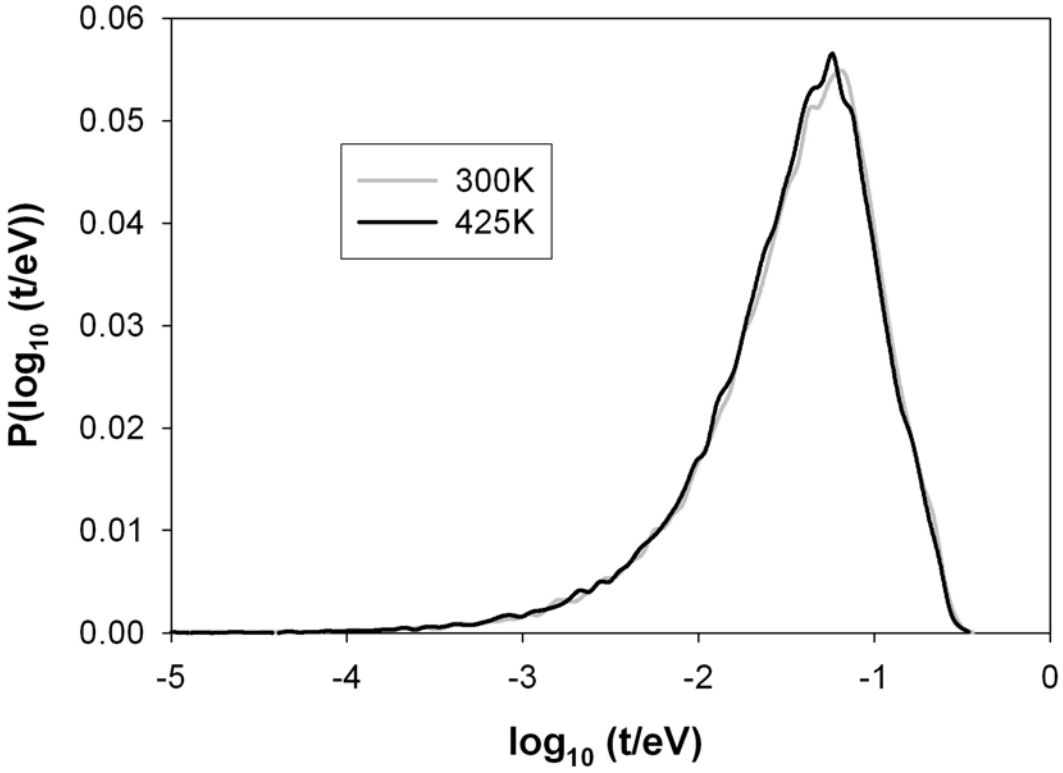

Figure 5 Olivier et al.

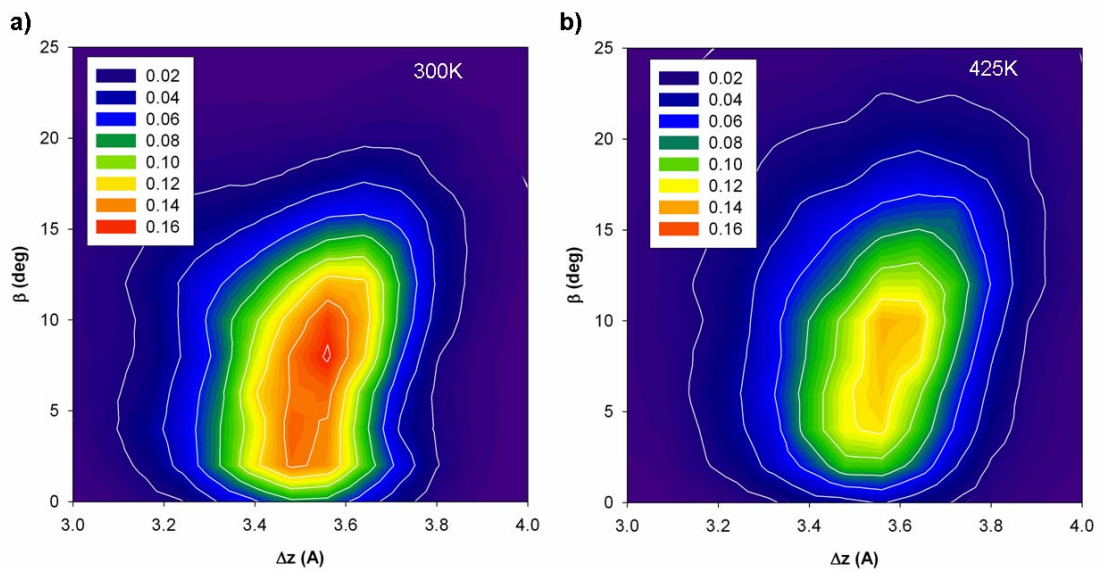

Figure 6 Olivier et al.

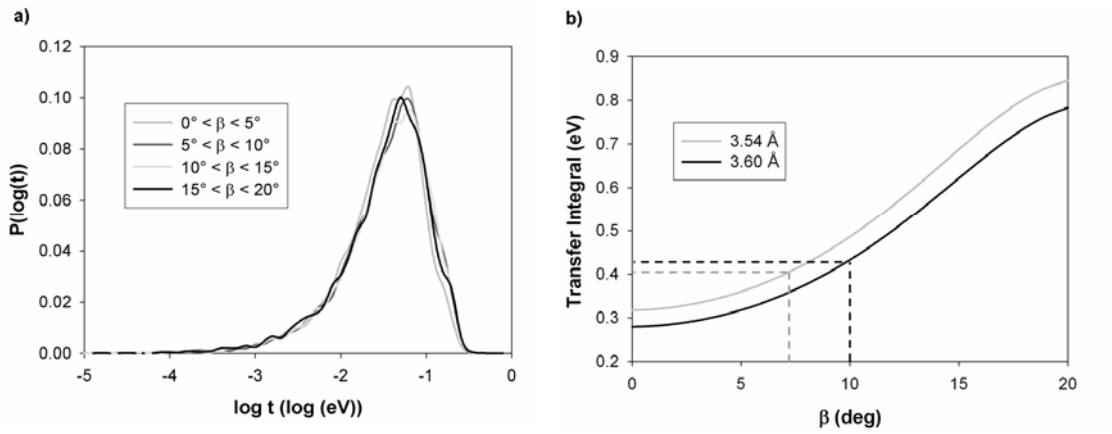

Figure 7 Olivier et al.

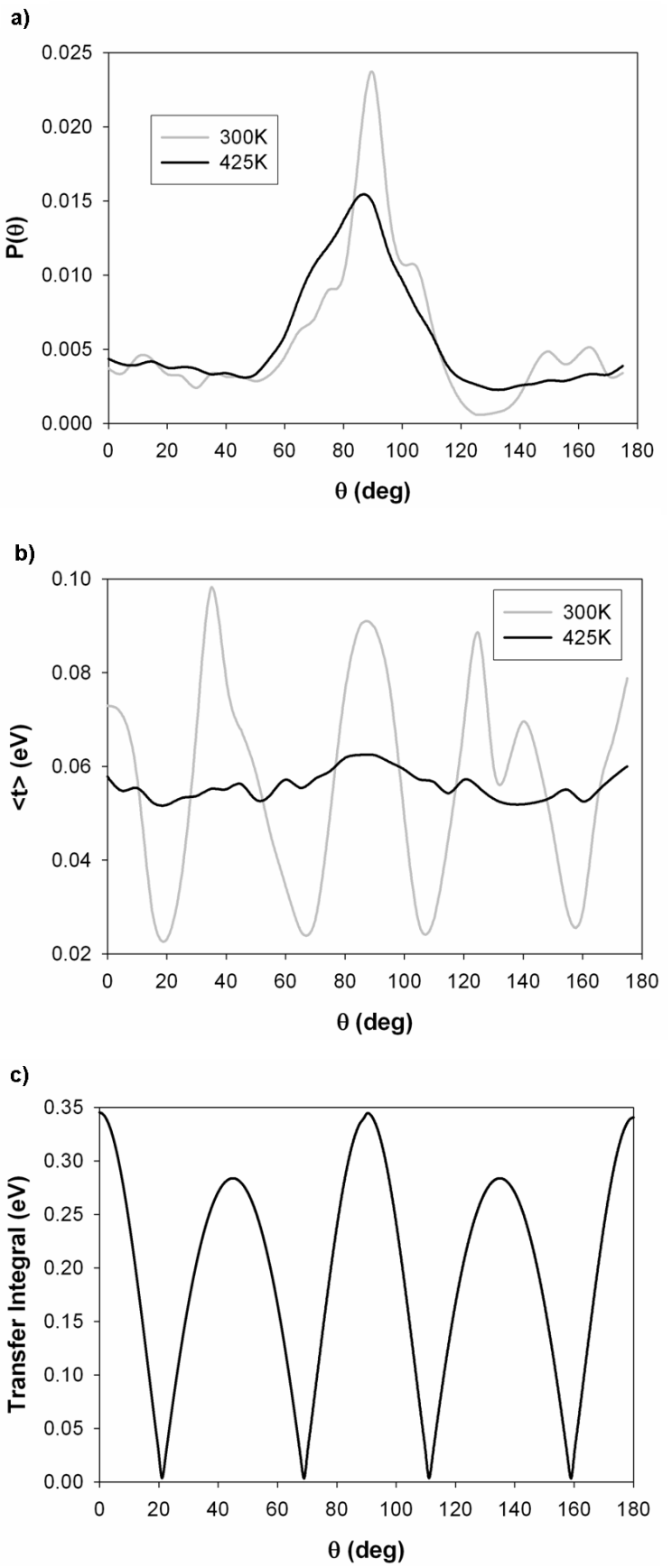

Figure 8 Olivier et al.

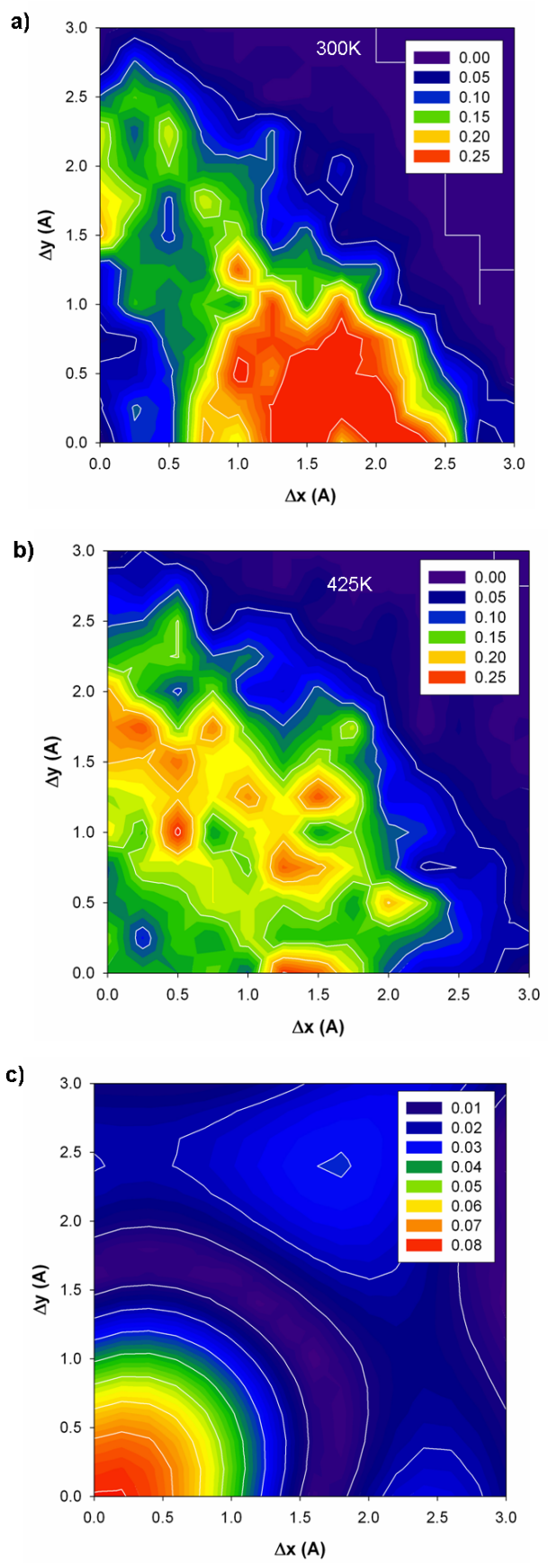

Figure 9 Olivier et al.

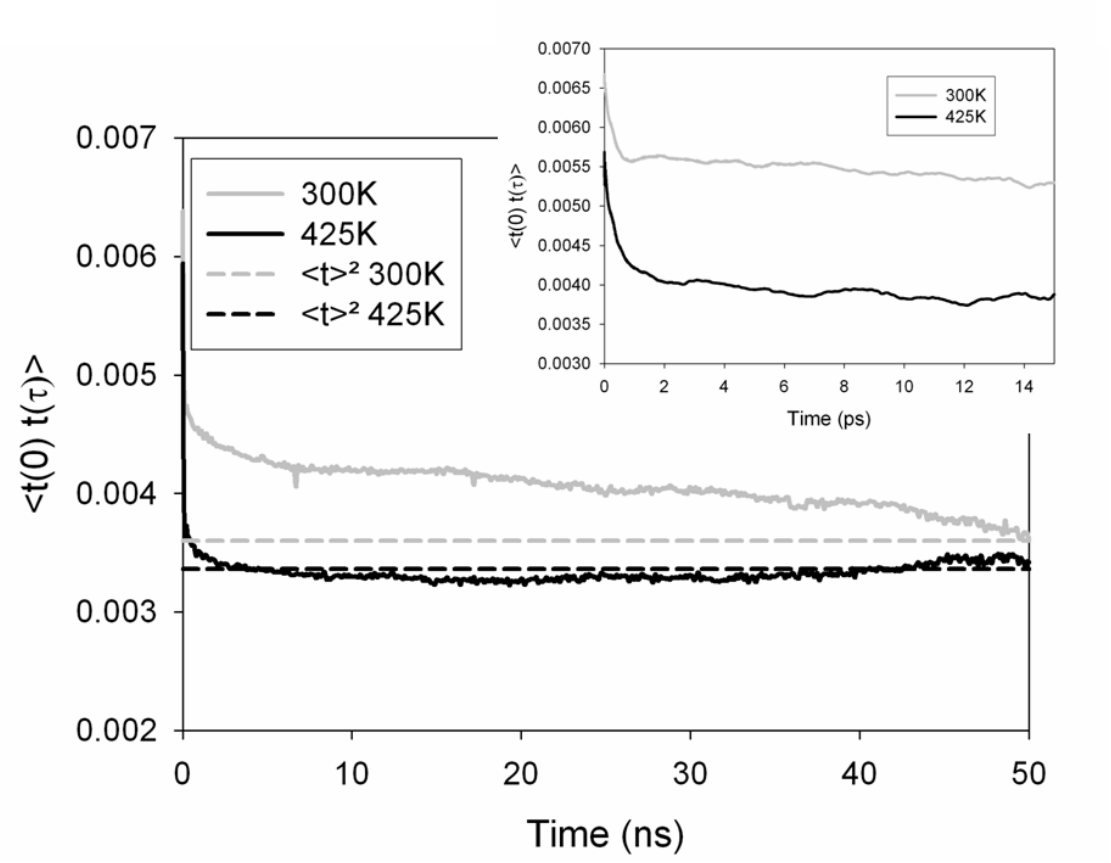

Figure 10 Olivier et al.

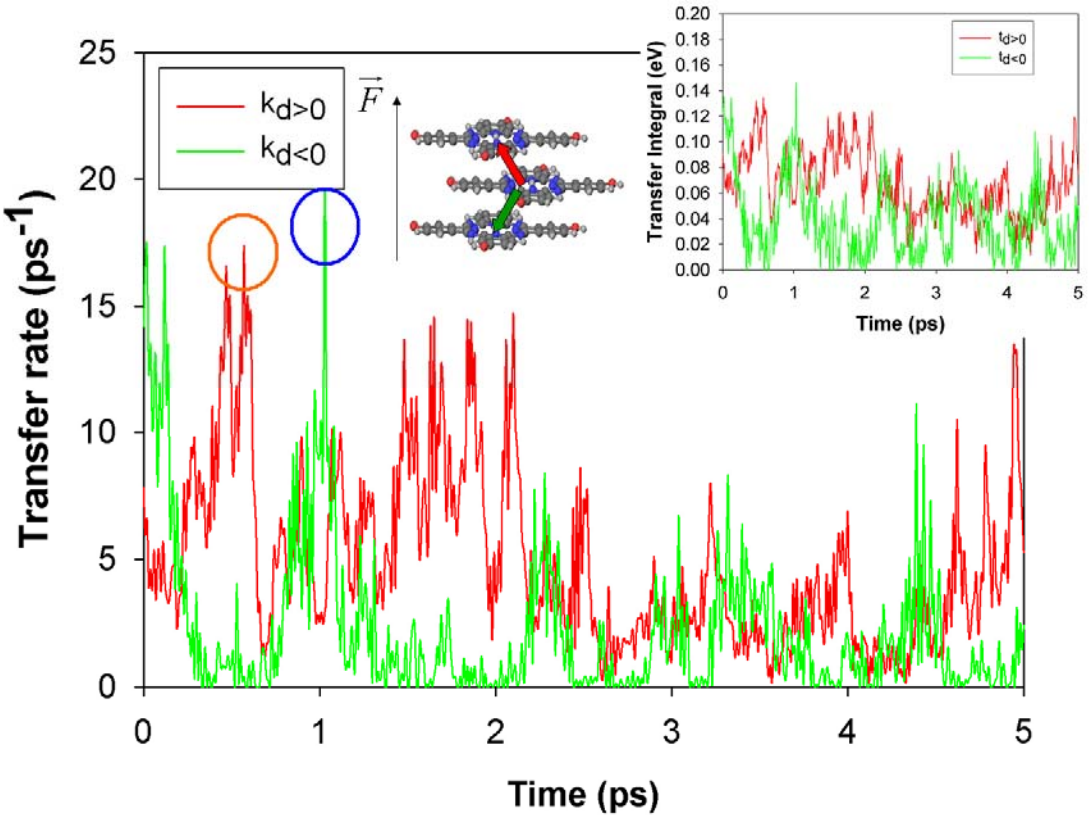

Figure 11 Olivier et al.